



# Methane, carbon dioxide, hydrogen sulfide, and isotopic ratios of methane observations from the Permian Basin tower network

Vanessa C. Monteiro<sup>1</sup>, Natasha L. Miles<sup>1</sup>, Scott J. Richardson<sup>1</sup>, Zachary Barkley<sup>1</sup>, Bernd J. Haupt<sup>2</sup>, David Lyon<sup>3</sup>, Benjamin Hmiel<sup>3</sup>, and Kenneth J. Davis<sup>1</sup>

<sup>1</sup>Department of Meteorology and Atmospheric Science, The Pennsylvania State University, University Park, 16802, PA, USA

<sup>2</sup>Earth and Environmental Systems Institute, The Pennsylvania State University, University Park, 16802, PA, USA

<sup>3</sup>Environmental Defense Fund, Austin, TX, USA

**Correspondence:** Natasha L. Miles ([nmiles@psu.edu](mailto:nmiles@psu.edu))

Received: 25 January 2022 – Discussion started: 4 February 2022

Revised: 13 April 2022 – Accepted: 16 April 2022 – Published: 20 May 2022

**Abstract.** We describe the instrumentation, calibration, and uncertainty of the network of ground-based, in situ, cavity ring down spectroscopy (CRDS) greenhouse gas (GHG) measurements deployed in the Permian Basin. The primary goal of the network is to be used in conjunction with atmospheric transport modeling to determine methane emissions of the Delaware sub-basin of the Permian Basin oil and natural gas extraction area in Texas and New Mexico. Four of the measurements are based on tall communications towers, while one is on a building on a mountain ridge, with the recent addition of a small tower at that site. Although methane ( $\text{CH}_4$ ) is the primary species of interest, carbon dioxide ( $\text{CO}_2$ ), hydrogen sulfide ( $\text{H}_2\text{S}$ ), and the isotopic ratio of methane ( $\delta^{13}\text{CH}_4$ ) are also reported for a subset of the sites. Measurements were reported following the WMO X2004A scale for  $\text{CH}_4$  and the WMO X2019 scale for  $\text{CO}_2$ . CRDS instruments were calibrated for  $\text{CH}_4$  and  $\text{CO}_2$  in the laboratory prior to deployment. For  $\text{H}_2\text{S}$ , data were offset-corrected using the minimum 40 min running mean value of the day, and for  $\delta^{13}\text{CH}_4$ , calibrations were based on laboratory data. We describe the characteristics of the dataset with a set of illustrative analyses. Methane and carbon dioxide showed strong seasonality, with a well-defined diurnal cycle during the summer, which was opposed to the winter, when a diurnal cycle was absent.  $\text{CH}_4$  enhancements to the background, during the winter, are up to twice the summer values, which is attributed to the changes in boundary layer depth and wind speed. The largest  $\text{CH}_4$  enhancements occurred when winds blow from the center of the Delaware sub-basin, where most of the methane emissions come from. The magnitude of enhancements of  $\text{CO}_2$  did not present seasonality.  $\text{H}_2\text{S}$  enhancements indicated a potential source northeast of the tower (Hobbs, New Mexico) where the inlet is installed. Isotopic ratios of methane indicated that oil and natural gas extraction is the source of local methane in the region. The hourly-averaged data, starting on 1 March 2020 and described in this paper, are archived at The Pennsylvania State University Data Commons at <https://doi.org/10.26208/98y5-t941> (Monteiro et al., 2021).

## 1 Introduction

Emissions of methane ( $\text{CH}_4$ ), such as from oil- and natural-gas-producing regions, are an environmental concern since  $\text{CH}_4$  is a greenhouse gas with a global warming potential 28–36 times larger than that of carbon dioxide ( $\text{CO}_2$ ) over a 100-year period, and 80 times larger than  $\text{CO}_2$  over a 20-year period (IPCC, 2021). This large difference in radiative forcing is a result of the relatively short atmospheric lifetime of  $\text{CH}_4$  ( $\sim 10$  years) compared to  $\text{CO}_2$  (lifetime of roughly hundreds or thousands of years, IPCC, 2021). As a result of its strong short-term impact, reductions in  $\text{CH}_4$  emissions are an efficient way to quickly reduce radiative forcing. According to Ocko et al. (2021), full implementation of all methane abatement technologies that are already technically feasible could cut anticipated global methane emissions in 2030 by 57 %, and global-mean average methane warming rates between 2030 and 2050 would consequently be reduced by 26 %.

About 60 % of the global  $\text{CH}_4$  budget arises from anthropogenic emissions (Saunio et al., 2020). Some of these emissions are fairly well-known since they are large point sources amenable to direct emissions monitoring (e.g., coal mines) (Kirchgessner et al., 2000). Some are relatively diffuse, large-area, low-intensity sources such as agricultural activities (Carlson et al., 2017; Moraes and Fadel, 2013) and leaks inside homes and buildings (Wennberg et al., 2012). A large component of anthropogenic emissions, however, comes from relatively compact, high-intensity, regional sources such as oil and gas (O&G) production basins (Alvarez et al., 2018; Maasackers et al., 2019; Pandey et al., 2019; Schwietzke et al., 2016). O&G-producing regions include numerous point sources covering a wide range of expected emissions (e.g., well pads and processing plants) and more diffuse sources such as gathering pipelines, sometimes intermingled with other methane sources such as livestock. Thus, O&G emissions are large in magnitude, and often highly uncertain. In addition, O&G production in the United States has increased dramatically since around 2005, driven primarily by hydraulic fracturing and horizontal drilling (Alvarez et al., 2012). This expansion of O&G production has prompted an increasing interest in monitoring of methane emissions from O&G basins on regional scales for the purpose of possible regulations and commercial incentives for operators to prove low emissions.

Atmospheric  $\text{CH}_4$  measurements can reduce uncertainty in  $\text{CH}_4$  emissions by providing “top-down” assessments of emissions. Top-down estimates are based on empirical data and atmospheric scientific methods, opposed to “bottom-up” approaches, which use an inventory approach and extrapolate regional emissions from smaller spatial scale measurement data as a component. The top-down emissions estimates can be compared with and used to improve more traditional accounting-based or inventory methods (e.g., Maasackers et al., 2016; U.S. EPA, 2019). Emissions of  $\text{CH}_4$  in the US

derived from atmospheric data have differed significantly from inventory assessments (Alvarez et al., 2018; Turner et al., 2015; Barkley et al., 2019b, 2021; Zhang et al., 2020), showing the importance of such independent data. Many past atmospheric studies of  $\text{CH}_4$  have used aircraft data to quantify emissions from O&G production basins (Baray et al., 2018; Barkley et al., 2017, 2019a,b; Karion et al., 2015; Schwietzke et al., 2017) and cities (Cambaliza et al., 2014; Conley et al., 2016; Heimbürger et al., 2017; Plant et al., 2019). Automobile-based measurements (e.g., Caulton et al., 2019; Omara et al., 2016; Robertson et al., 2020) have also been used to great advantage to characterize emissions from individual O&G production sites. Aircraft and automobile measurements, which are spatially rich in information content, are typically short-term in nature. Even extended airborne campaigns (e.g., Heimbürger et al., 2017; Barkley et al., 2021) have limited availability to date to capture temporal trends in basin- or city-scale emissions.

Observations of atmospheric methane are sparse, with limited in situ sites located mostly in North America and Europe (e.g., Andrews et al., 2014; Karion et al., 2015). Satellite-based measurements such as the Greenhouse Gas Observing Satellite (GOSAT) and the Tropospheric Monitoring Instrument (TROPOMI) data provide global remote sensing of column atmospheric methane ( $\text{XCH}_4$ ; e.g., Qu et al., 2021) and will strengthen our understanding of the global methane budget, but quantification of the level of bias and uncertainty in methane emissions estimates as a function of conditions known to affect satellite retrievals is critical. Tower- and building-based in situ networks measuring  $\text{CH}_4$  dry mole fractions within the boundary layer have been used to quantify urban emissions (e.g., Lamb et al., 2016; McKain et al., 2015; Yadav et al., 2019; Sargent et al., 2021). Chan et al. (2020) used in situ monitoring to quantify methane emissions for the Western Canadian Sedimentary O&G Basin, and Lin et al. (2021) quantified methane emissions from the Uinta O&G Basin. Here, we present observations from a tower-based atmospheric monitoring network designed to track  $\text{CH}_4$  emissions from the Delaware sub-basin of the Permian Basin.

The Permian Basin is the largest oil-producing region in the United States, and the second largest natural-gas-producing region, accounting for 40 % of the US oil production and 15 % of the US natural gas production (Enerverus Drillinginfo, 2021). The Permian Basin is also a high-emission US oil- and natural-gas-producing region according to satellite observations (Zhang et al., 2020), with a natural gas production normalized loss rate of 3.7 %. Emissions of methane are associated with midstream processing (e.g., Mitchell et al., 2015), flares (e.g., Allen et al., 2016), and with low-producing marginal wells (e.g., Deighton et al., 2020).

This tower-based network was deployed in late February 2020, just prior to the COVID-19 pandemic lockdown in the United States. The data reported here stop on 9 November 2021, but the network is still in operation. Using these tower

observations alongside aircraft measurements, satellite observations, and model estimates, Lyon et al. (2021) found a correlation between decreasing oil prices and the CH<sub>4</sub> emissions during the COVID-19 lockdown (March–April 2020) and hypothesized that under normal conditions, production exceeds the midstream capacity, resulting in more venting and flaring, and consequently higher methane emissions.

The primary purpose of this paper is to describe the high-accuracy mole fraction measurements of CH<sub>4</sub> including the network and site characteristics (Sect. 2); instrumentation used for data collection (Sect. 3); and the associated calibration, processing, uncertainties, and data coverage (Sect. 3). We also describe opportunistic measurements of CO<sub>2</sub>, hydrogen sulfide (H<sub>2</sub>S), and the methane isotope ratio ( $\delta^{13}\text{CH}_4$ ), which are of interest but are not the focus of this network. Section 4 presents summary data for all gases (CH<sub>4</sub>, CO<sub>2</sub>, H<sub>2</sub>S, and  $\delta^{13}\text{CH}_4$ ) to date, and an example analysis of each gas. The example analyses include diurnal cycles and enhancements for CH<sub>4</sub>, CO<sub>2</sub>, and H<sub>2</sub>S, and the determination of source isotopic signature using  $\delta^{13}\text{CH}_4$  and CH<sub>4</sub> measurements. We have included brief methods for these analyses in each subsection, rather than a separate section for methods.

## 2 Network and site characterization

The Permian Basin in situ tower observation network includes five monitoring stations in the Delaware sub-basin (Fig. 1a, Table 1): Carlsbad Caverns National Park (CARL), Maljamar (MALJ), Hobbs (HOBB), Notrees (NOTR), and Fort Stockton (FORT). The instruments installed at the stations measure methane concentrations continuously, beginning on 1 March 2020. The towers encompass an area of approximately 160 km × 220 km. Of the monitoring stations, four are communications towers with gas inlets installed at 91–134 m a.g.l. (height above ground level). Due to the lack of availability of a tower, the instrumentation at the Carlsbad location was initially deployed on a rooftop (4 m a.g.l.). On 13 May 2021, the instrumentation was moved to a 9 m tower approximately 250 m to the east of the original location. The Carlsbad site is at 1349 m above sea level on a mountain ridge, significantly higher than the surroundings' elevation (e.g., the elevation in White City, 6 km to the east of Carlsbad tower, is 1112 m a.s.l.). The location is within Carlsbad Caverns National Park and hence is buffered from oil and gas infrastructure immediately adjacent to the measurement site. At Hobbs, additional inlets were installed at 2 m a.g.l. and inside the building at the base of the tower.

The prevailing wind direction in the region varies seasonally (Fig. 1b). During the winter (i.e., December, January, February, DJF), the wind most often comes from SW–W directions, while during the summer (i.e., June, July, August, JJA), the prevailing direction is from the south. This behavior makes the measurements obtained from Carlsbad (during winter) and Fort Stockton (during summer) the most likely

background sites since most of the time they are not directly impacted by CH<sub>4</sub> emissions originating from the oil and gas fields located within the Delaware sub-basin to the east and north of these towers, respectively.

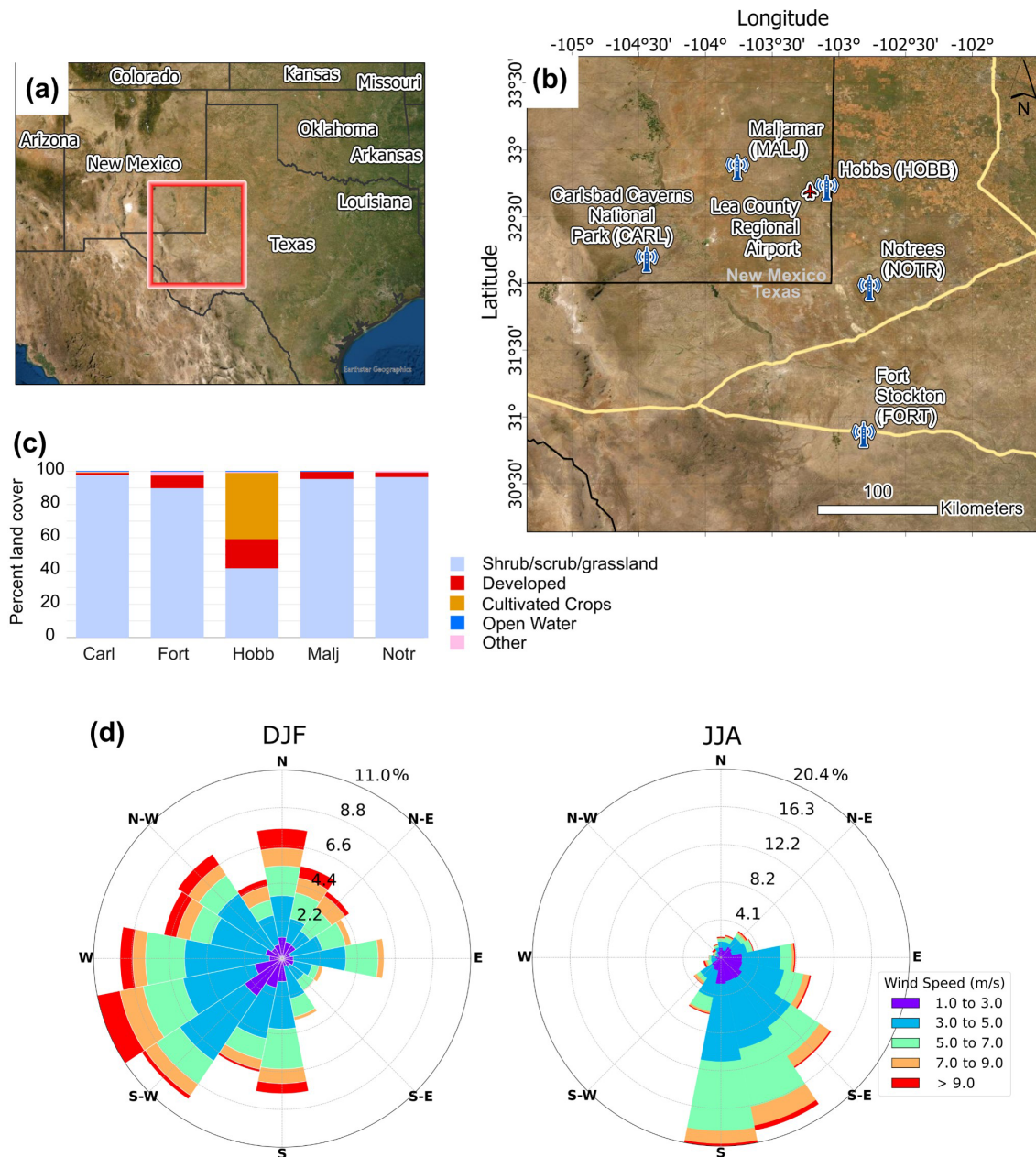
New Mexico and Texas are within a region of extensive production of oil and natural gas, and the landscape surrounding the towers are mostly shrub, scrub, and grassland (Fig. 1c). Hobbs is the only site with significant agricultural and urban land cover. Within a 10 km radius of the Hobbs tower, the landscape is ~ 40 % shrub, scrub, and grassland; ~ 40 % cultivated crops (to the east of the tower); and ~ 20 % urban area (to the west of the tower). These relatively simple surroundings in terms of methane emissions simplify the task of isolating emissions from the basin's O&G infrastructure, which accounts for > 90 % of methane emissions in the Permian Basin (Maasackers et al., 2016).

## 3 Instrumentation, calibration measurements, and uncertainty

### 3.1 Instrumentation, sampling details, and calibration

Mole fraction measurements were made with wavelength-scanning cavity ring down spectroscopic (CRDS) instruments (Picarro, Inc., models G2301, G2401, G2204, and G2132-i). The primary species of interest for this network was CH<sub>4</sub>. Most of the instruments also reported CO<sub>2</sub>, one reported H<sub>2</sub>S, and at various locations and time periods  $\delta^{13}\text{CH}_4$  was reported. Instrument failures necessitated multiple exchanges of instrumentation for repairs.

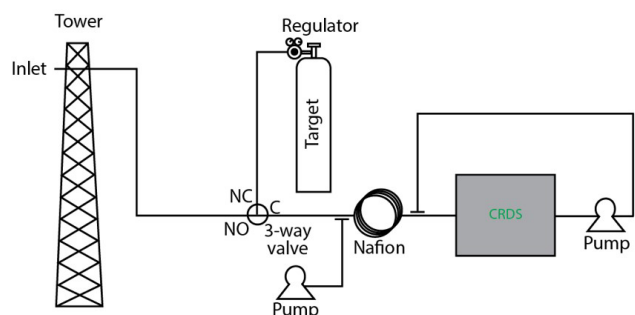
The in situ sampling method was similar to the procedures described in Richardson et al. (2017), and the schematic for the systems as deployed in the field is shown in Fig. 2. Collocated at the top sampling level of each tower were two 1/4 in. (0.64 cm) OD Synflex 1300 (Eaton Corp.) tubes with rain shields to prevent liquid water from entering the sampling line. Air was drawn down from the inlet on the tower, through the Nafion dryer (MD Series, Permapure LLC, 24 in. (61 cm) to 96 in. (244 cm) lengths, depending on availability), into the CRDS instrument for analysis, and then used as the purge gas in the Nafion dryer (i.e., re-flux method). Field calibration tank gas was introduced upstream of the dryer, humidifying the calibration gas via 1/8 in. (0.32 cm) OD stainless steel tubing. Scott Specialty Gas (now Air Liquide) two-stage regulators (part number 51-14 A-590, similar to Air Liquide, part number Q1-14B-590) were used for sampling the field calibration tanks. Three-way solenoid valves (part number 091-0094-900, Parker Hannifin Corp.) were used to switch between sample and field calibration gas. For the Hobbs site, the top level was sampled for 40 min of each hour and the lower levels were each sampled for 10 min. We ignored 4 min after every transition for equilibration. Correction factors, based on factory default H<sub>2</sub>O factors, were applied to adjust the CH<sub>4</sub> and CO<sub>2</sub> values for the effects of the remaining water vapor (Rella et al., 2013).



**Figure 1.** Location of the Permian Basin network towers and land cover characteristics. **(a)** Area, highlighted in red, in New Mexico and Texas where the Permian Basin tower network is located. **(b)** Five towers located in New Mexico and Texas as part of the Permian Basin towers network and the Lea County Regional Airport location. The towers continuously measure  $\text{CO}_2$ ; HOBB measures  $\text{H}_2\text{S}$ ; and MALJ and NOTR measure  $\delta^{13}\text{C}\text{CH}_4$ . **(c)** Percent land cover from 2016 National Land Cover Database (MRLC, 2019) within 10 km radius of each tower. Most of the area surrounding the towers is covered by shrub, scrub, and grassland. Some land cover types were grouped for simplicity, e.g., “developed” corresponds to all developed categories (high density, medium density, low density, and open space), and “other” corresponds to evergreen forest, barren land, woody wetlands, and emergent herbaceous wetlands. **(d)** Wind rose showing the prevailing wind direction during winter months, i.e., December, January, February (DJF), and summer months, i.e., June, July, August (JJA), for the years of 2020 and 2021. The percent scale (radial axis) shows the frequency of the wind blowing from a specific direction. Weather data were obtained from Lea County Regional Airport in Hobbs, NM (retrieved from Iowa Environmental Mesonet; IEM, 2021). Known well locations are shown in Fig. 7. Credits for base map: Esri, DigitalGlobe, GeoEye, Earthstar Geographics, CNES/Airbus DS, USDA, USGS, AeroGRID, IGN, and the GIS User Community.

**Table 1.** Locations, inlet heights, species measured, and installation dates of in situ tower-based measurements in the Permian Basin.

Site	Latitude	Longitude	Elevation (m a.s.l.)	Inlet height (m a.g.l.)	Species measured	Install date
Carlsbad Caverns National Park (CARL)	32.1782° N (prior to 13 May 2021); 32.1783° N (thereafter)	104.4434° W (prior to 13 May 2021); 104.4406° W (thereafter)	1349	4, 9	CH <sub>4</sub> , CO <sub>2</sub>	29 Feb 2020
Fort Stockton (FORT)	30.8666° N	102.8150° W	987	128	CH <sub>4</sub> , CO <sub>2</sub> , $\delta^{13}\text{CH}_4$	29 Feb 2020
Hobbs (HOBB)	32.7135° N	103.0913° W	1103	Inside (0.5), 2, 91	CH <sub>4</sub> , CO <sub>2</sub> , H <sub>2</sub> S	27 Feb 2020
Maljamar (MALJ)	32.8671° N	103.7608° W	1310	134	CH <sub>4</sub> , CO <sub>2</sub> , $\delta^{13}\text{CH}_4$	27 Feb 2020
Notrees (NOTR)	31.9657° N	102.7699° W	1015	91	CH <sub>4</sub> , CO <sub>2</sub> , $\delta^{13}\text{CH}_4$	28 Feb 2020

**Figure 2.** Schematic of the systems deployed in the field. The Hobbs site has additional inlets at 2 m a.g.l. and inside the building, and associated valves as shown in Fig. 2b in Richardson et al. (2017).

The measurements are reported on the World Meteorological Organization (WMO) X2004A scale for CH<sub>4</sub>, and the WMO X2019 scale for CO<sub>2</sub>. H<sub>2</sub>S and  $\delta^{13}\text{CH}_4$  (tied to the Vienna Pee Dee Belemnite (VPDB) scale) are reported, but with limited calibration. The G2301 and G2401 CRDS instruments (Picarro, Inc.) were calibrated for CH<sub>4</sub> and CO<sub>2</sub> in the laboratory prior to deployment using four NOAA (National Oceanic and Atmospheric Administration) tertiary standards, ranging between 1790 and 2350 ppb CH<sub>4</sub>, and 360 and 450 ppm CO<sub>2</sub>, sampling each tank at least 5 min after equilibration, and repeating at least once. We characterized the G2132-i and G2204 instruments using 2–4 tanks and applied the calibration in the post-processing stage.

To calibrate the field tanks prior to deployment, we first calibrated a dedicated laboratory CRDS instrument as above. We then used the CRDS instrument to sample each field calibration tank and assigned the mean to each tank. Field calibration tanks (size N80, expected to last 12–18 months,

and listed in Table 2) were sampled nominally every 23 h for 6 min for G2301, G2401, and G2204 instruments, and every 6 h for 20 min for G2132-i instruments, but adjustments were occasionally made to limit field calibration gas usage. After each transition between calibration gas and atmospheric sample, 4 min of data are ignored. An offset correction was applied daily. One disadvantage of this procedure is the potential introduction of tank drift to the data, but tank drift for CH<sub>4</sub> has not been observed (Andrews et al., 2014). Allan deviations were < 0.2 ppb CH<sub>4</sub> and 0.02 ppm CO<sub>2</sub> for 2 min samples for the G2301 and G2401 instruments (Yver Kwok et al., 2015), and 0.1 ppb CH<sub>4</sub> and 0.1 ppm CO<sub>2</sub> for the ~ 1 h sample for the G2132-i instruments (Miles et al., 2018), and thus the noise for these instruments for the calibration cycles is insignificant. Ideally, more than one tank would be sampled at each site, but this was not practical for this network. Data from the first 4 min after a transition between gases was discarded. Flow rates for G2301, G2401, and G2204 instruments were about 240 cm<sup>3</sup> min<sup>-1</sup>, whereas the flow rates for the G2132-i instruments were about 30 cm<sup>3</sup> min<sup>-1</sup>. Residence time from the top of the tower to measurement was 6 to 9 min for the G2301, G2401, and G2204 instruments and 45 to 70 min for the G2132-i. For the Carlsbad site sampling from a rooftop, then a 9 m tower, residence times were < 1 min. The data were adjusted to report the sampling time, rather than the measurement time, taking into account the residence times.

We offset-corrected the H<sub>2</sub>S data using the minimum 40 min running mean value of the day (assumed to be zero) instead of a field calibration tank because a tank was not available for an extended period of the deployment. For the period for which a field calibration was available, the mean was within 0.05 ppb of the lowest H<sub>2</sub>S throughout the day, which was small compared to the observed signals. The stan-

**Table 2.** Table of calibration cylinders used at the Permian Basin tower network sites. Within each site, the cylinders are listed in order of use.

Location	Cylinder	Dates	CH <sub>4</sub> (ppb, x2004A)	CO <sub>2</sub> (ppm, x2019)	$\delta^{13}\text{CH}_4$ (‰)*	CO (ppb, x2014A)
Carlsbad	LL120758	29 Feb 2020– 14 May 2021	1976.1	420.12	N/A	125.1
Carlsbad	LL120763	14 May 2021– 9 Nov 2021	2031.0	426.57	N/A	141.3
Fort Stockton	LL120783	29 Feb 2020– 15 May 2021	1977.8	419.79	N/A	126.6
Fort Stockton	LL120762	29 Feb 2020– 15 May 2021	1976.4	419.94	N/A	N/A
Fort Stockton	LL55866	16 May 2021– 9 Nov 2021	2351.6	430.40	N/A	304.7
Hobbs	LL120792	27 Feb 2020– 9 Jun 2020	2032.9	424.56	N/A	N/A
Hobbs	LL120780	10 Jun 2020– 15 Sep 2020	1974.3	419.90	N/A	N/A
Hobbs	LL108056	16 May 2021– 9 Nov 2020	2110.6	410.24	N/A	N/A
Maljamar	LL120782	8 Jun 2020– 9 Nov 2021	1974.0	419.54	−46.5	N/A
Maljamar	LL120789	8 Jun 2020– 9 Nov 2021	2028.5	425.78	−46.5	145.3
Notrees	LL120799	28 Feb 2020– 14 May 2021	2035.5	425.91	N/A	151.1
Notrees	LL120795	15 May 2021– 9 Nov 2021	2022.4	424.66	−47.0	N/A

\*  $\delta^{13}\text{CH}_4$  values are based on field calibrations of the cylinders. N/A: not available.

dard deviation of the instrument drift based on the field calibration tank was  $\pm 0.43$  ppb throughout the period June–August 2021. A calibration tank with known non-zero H<sub>2</sub>S mole fraction was not available, so we were not able to assess the calibration slope. We did not apply any correction to the H<sub>2</sub>S for water vapor.

We applied  $\delta^{13}\text{CH}_4$  calibrations based on laboratory data (Miles et al., 2018) and tested with a tank characterized by the Institute of Arctic and Alpine Research (INSTAAR) prior to deployment, but field calibration tanks with varying  $\delta^{13}\text{CH}_4$  values were not available for this network. A daily offset-correction was applied to the  $\delta^{13}\text{CH}_4$ , using a field-calibrated tank. The uncertainty is estimated to be 1‰, compared with 0.15‰ uncertainty reported by Miles et al. (2018) when utilizing multiple field calibration tanks.

### 3.2 Uncertainty

The uncertainty of the reported hourly values for CH<sub>4</sub> and CO<sub>2</sub> include contributions from measurement uncertainty, extrapolation, and water vapor (Andrews et al., 2014; Verhulst et al., 2017; Karion et al., 2020). The measurement uncertainty is composed of uncertainties attributable to short-term precision, calibration baseline, and scale. We assessed the effects of instrument short-term precision and drift between calibration cycles (i.e., calibration baseline) using a 31 d running standard deviation of the daily tank residuals, reporting the  $2\sigma$  value. Typical values vary with instrument type (e.g., 0.6 ppb CH<sub>4</sub> and 0.06 ppm CO<sub>2</sub> for G2301, 1.0 ppb CH<sub>4</sub> and 0.18 ppm CO<sub>2</sub> for G2132-i, and 6.8 ppb CH<sub>4</sub> for G2204). Scale (i.e., tank assignment) uncertainty is set to 1.0 ppb CH<sub>4</sub> and 0.06 ppm CO<sub>2</sub>, following Andrews et al. (2014). Ideally, a target tank is used to independently assess the measurement uncertainty, but for this network only one tank was deployed at each site.

Because we performed a full calibration of the instruments using four NOAA-calibrated tanks prior to deployment (and upon any factory repairs), extrapolation error is expected to be small and is not specifically reported here. Round-robin-style tests have indicated that if full calibrations are performed at least every 2 years, in addition to a daily single-point adjustment, differences from known values are within 1 ppb CH<sub>4</sub> and 0.1 ppm CO<sub>2</sub> (Richardson et al., 2017).

We assessed the uncertainty due to water vapor based on the difference in water vapor mole fraction between the dried sample and the humidified field calibration gas. The difference varied due to length of the Nafion dryer, building temperature, and instrument flow rate but was typically between 0.05 % and 0.7 % H<sub>2</sub>O. No drying was employed at the Hobbs site for March 2020–May 2021, during which time the water vapor was up to 2 %. Errors in the coefficients used to determine the water vapor correction can vary by instrument and are the largest contributor for cases with moderate or no drying. Rella et al. (2013) showed that errors associated with the water vapor correction, even with no drying, are less than WMO compatibility goals for CO<sub>2</sub> and CH<sub>4</sub> (0.1 ppm CO<sub>2</sub> and 2 ppb CH<sub>4</sub>) if instrument specific correction factors are determined periodically. The error associated with relying on general correction factors (as used here) is up to 0.25 ppm CO<sub>2</sub> and 2.0 ppb CH<sub>4</sub> for 3 % water vapor. We have therefore assumed the uncertainty due to the water vapor correction to be a linear function between these values and no error at 0 % water vapor. The uncertainty due to the water vapor correction when drying was 0.00–0.06 ppm CO<sub>2</sub> and 0.0–0.6 ppb CH<sub>4</sub>. For the period without drying at the Hobbs site, the uncertainty was up to 0.17 ppm CO<sub>2</sub> and 1.7 ppb CH<sub>4</sub>.

The initial instrument at the Notrees site did not report water vapor for 1 March–27 July 2020 due to a laser problem. For that period, we applied a water correction and uncertainty based on the subsequent mean and standard deviation of the water vapor ( $0.53 \pm 0.19$  %). The uncertainty in the water vapor value led to uncertainty in the CO<sub>2</sub> of  $\sim 1.1$  ppm CO<sub>2</sub> and 5 ppb CH<sub>4</sub> for this period. For 28 July–31 December 2020, the instrument did report H<sub>2</sub>O, but CH<sub>4</sub> and CO<sub>2</sub> uncertainty due to noise continued to be higher (2.3 ppb CH<sub>4</sub> and 0.58 ppm CO<sub>2</sub>) than subsequent values for this instrument (0.4 ppb CH<sub>4</sub> and 0.04 ppm CO<sub>2</sub>). The intra-network CH<sub>4</sub> differences across the Delaware Basin were 135 ppb (winter) and 51 ppb (summer), whereas the CO<sub>2</sub> differences were 0.8 ppm (winter) and 1.2 ppm (summer) (Sect. 4.3). Thus, the CH<sub>4</sub> uncertainty during this period was small compared to intra-network differences, but nearly the same magnitude for CO<sub>2</sub>. Consequently, we flagged CO<sub>2</sub> for 1 March–31 December 2020 as unsuitable for use and replaced the mole fractions with a placeholder value (NaN). The instrument was replaced on 15 May 2021.

The results for these contributions to the uncertainty, summed in quadrature, are shown in Fig. 3. The uncertainty ( $2\sigma$ ) of the G2301 and G2132-i instruments when operat-

ing normally is better than 1.5 ppb CH<sub>4</sub>. For CO<sub>2</sub>, the uncertainty is better than 0.07 ppm for the G2301 instruments and 0.30 ppm for the G-2132i instruments. Note that the Hobbs instrument does not measure CO<sub>2</sub> and that the uncertainty for CH<sub>4</sub> is larger due to the instrument type (G2204). Manufacturer precision specifications of the instrument model at this site indicate CH<sub>4</sub> precision for a 5 s sample of 2 ppb compared to the other instrument models used in this network (CH<sub>4</sub> precision for a 5 s sample of < 0.5 ppb).

H<sub>2</sub>S and  $\delta^{13}\text{CH}_4$  are reported in this dataset but are not the focus of this research. Since a field calibration tank with non-zero H<sub>2</sub>S was not available, we reported the manufacturer-specified precision of 1 ppb + 0.4 % H<sub>2</sub>S as an estimate of instrument uncertainty. The standard deviation of 2 months of quasi-daily field calibration data for the isotopic ratio of methane at the Maljamar site was 0.32 ‰. Because these instruments relied on a laboratory  $\delta^{13}\text{CH}_4$  calibration performed in 2015, there may be additional slope errors not captured by the single field calibration tank, and we have reported the uncertainty on the isotope ratio as 1 ‰.

## 4 Methane, carbon dioxide, hydrogen sulfide, and isotopic ratio of methane measurements

### 4.1 Data coverage

The data coverage of the hourly-averaged observations for each species for the Permian Basin tower network through the beginning of November 2021 is indicated in Fig. 4. For the period 9 June 2020–16 May 2021, a leak near the inlet to the instrument was identified at the Hobbs site. The field calibration tank emptied unusually quickly, and flow rates measured near the instrument inlet on a site visit indicated a leak. Although the leak is not apparent upon inspection of the data in isolation or via comparison with the other network sites, we have flagged these data as unsuitable for use and replaced them with a placeholder value (NaN) in an abundance of caution. The original data are, however, available online.

### 4.2 Diurnal cycle and seasonality

Composited means of hourly CH<sub>4</sub> and CO<sub>2</sub> mole fractions (averaged over summer and winter seasons) indicate clear seasonality (Fig. 5). The atmospheric boundary layer is typically deeper in the summer, which is consistent with the observed lower mole fractions of CH<sub>4</sub> and CO<sub>2</sub>, compared to the wintertime. Methane and carbon dioxide have a distinct diurnal cycle during the summer months, with the highest mole fractions between 10:00 and 15:00 UTC (night). In Texas the local time is UTC – 5, and in New Mexico it is UTC – 6. The observed CH<sub>4</sub> mole fraction in the summer is lowest at Fort Stockton, which is consistent with predominantly southerly winds (Fig. 1b) and the majority of the oil and natural gas facilities being to the northwest of this tower. During the winter months, when winds are predominantly

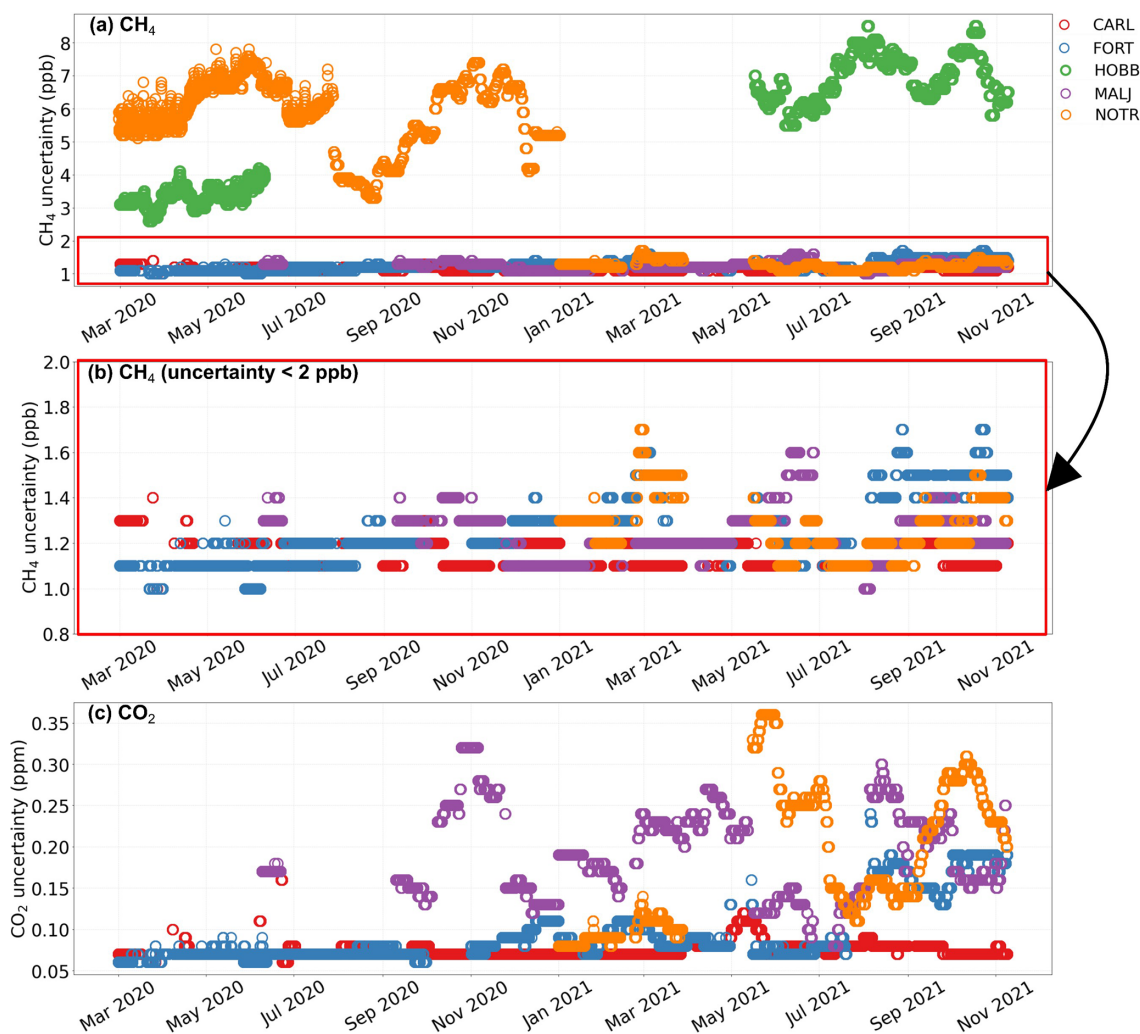


**Figure 3.** CH<sub>4</sub> and CO<sub>2</sub> uncertainties from March 2020–November 2021, at the five sites: Carlsbad (CARL), Fort Stockton (FORT), Hobbs (HOBBS), Maljamar (MALJ), and Notrees (NOTR). (a) CH<sub>4</sub> uncertainty. (b) CH<sub>4</sub> uncertainty close-up (< 2 ppb). (c) CO<sub>2</sub> uncertainty.

from the SW–W direction, the lowest CH<sub>4</sub> is measured at Maljamar on the northern edge of the network for most hours of the day. The diurnal amplitude in CO<sub>2</sub> is 1 ppm during the winter, compared to 5 ppm during the summer.

Due to data availability, the seasonality of H<sub>2</sub>S cannot be assessed. Hourly composites of the H<sub>2</sub>S mole fraction during the summer months show a clear diurnal cycle (Fig. 6). The concentrations at 91 m a.g.l. and inside the building have similar diurnal cycle signature and magnitude. On the other hand, 2 m a.g.l. presented the highest concentration and is significantly different from the 91 m a.g.l. observations. Filtration by the air conditioning system appears to have reduced the H<sub>2</sub>S mole fractions inside the building. While background levels of H<sub>2</sub>S are essentially zero, the mean H<sub>2</sub>S mole fraction at direct exposure level for humans (2 m a.g.l.) is on the order of 8 ppb around 12 UTC, which is 4 times larger than the levels observed inside the building and at 91 m a.g.l.. These levels of H<sub>2</sub>S are not a health concern

(OSHA, 2022) but do indicate the existence of an H<sub>2</sub>S source near the tower.

#### 4.3 Methane, carbon dioxide, and hydrogen sulfide enhancements

Atmospheric inversion techniques, used to estimate gas emissions, rely on accurate quantification of enhancements, which are defined as the difference between the tower network background, which may be defined in a variety of ways (e.g., Miles et al., 2017; Karion et al., 2021; Sargent et al., 2018), and the mole fraction observed at each tower. Typically, enhancements are calculated for afternoon hours, and here we defined afternoon hours from 20:00 to 23:00 UTC. To determine the enhancements, we averaged the afternoon mole fractions at each tower and obtained the background for CH<sub>4</sub> and CO<sub>2</sub> from the minimum averaged afternoon mole fraction of the entire network. Thus, each day has one value





**Figure 4.** Data availability and instruments used at each site. Inlet level (meters above ground level) is indicated beside the site name. **(a)** Methane (CH<sub>4</sub>) data availability at all sites. **(b)** Carbon dioxide (CO<sub>2</sub>) data availability. **(c)** Hydrogen sulfide (H<sub>2</sub>S) data availability. **(d)** Methane isotope (δ<sup>13</sup>C<sub>4</sub>) data availability. At the sites with more than one level of measurement (e.g., HOBB and CARL), all the levels operate using the same instrument at that site. Instruments replacements were made due to instrument failures at FORT, MALJ, and NOTR.

for the background, and each tower has one enhancement value per day. For H<sub>2</sub>S, we assumed that the background is zero since this gas is not expected to be found naturally in this region. We used the wind data from Lea International Airport in Hobbs and excluded directions from which the wind originated for five or fewer days during the analysis period (e.g., summer and winter months). Calm winds ( $< 1.6 \text{ m s}^{-1}$ ) were also excluded from the analysis.

Enhancements of methane have strong seasonality, with smaller enhancements during the summer months (Fig. 7a) when compared to the enhancement during the winter months (Fig. 7b). During the summer, there is intense surface heating in the region, and deep boundary layer depths, compared to the winter months when more stable atmospheric conditions and lower atmospheric boundary layer depths occur. The largest enhancements of CH<sub>4</sub> occur when the wind blows from the center of the Delaware sub-basin (Fig. 7), which is coincident with the high estimated emission rates of methane (Zhang et al., 2020).

The seasonality of methane observations is also apparent in the daily afternoon differences between the largest and smallest CH<sub>4</sub> mole fraction measured from the tower network from 1 March 2020 to 1 August 2021 (Fig. 8). While in summer months the afternoon differences do not exceed 150 ppb, in the winter months the differences reached more than 900 ppb. For the 30 d mean, the summer differences ranged from 50 to 100 ppb, and winter differences were twice the summer values and are usually between 150 and 200 ppb. Note that Fig. 5 shows averaging across a 3-month period, while Figs. 7 and 8 show daily maximum and minimum differences. In the summer, FORT is the site with minimum afternoon CH<sub>4</sub> 50 % of the days, but during the winter, the site exhibiting the minimum CH<sub>4</sub> is much less consistent, with CARL at 29 %, FORT at 27 %, and MALJ at 20 % of the days. Thus, while the daily afternoon intra-network differences are large in the winter (Fig. 8), the mean difference between sites when averaged over 3 months is 40 ppb (Fig. 5b).

Even though the composite diurnal cycle of CO<sub>2</sub> mole fractions presented some seasonality (Fig. 5c and d), the

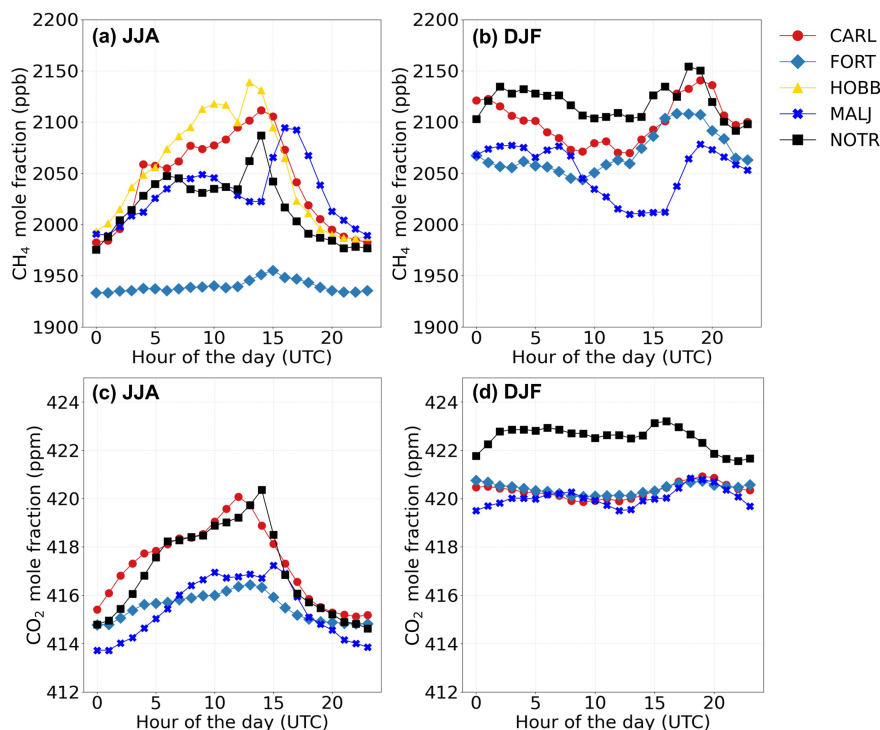


**Figure 5.** Diurnal cycle of species measured at the Permian Basin network during the winter months (December, January, February), and during the summer months (June, July, August). (a) Diurnal cycle of CH<sub>4</sub> during winter. (b) Diurnal cycle of CH<sub>4</sub> during summer. (c) Diurnal cycle of CO<sub>2</sub> during winter. (d) Diurnal cycle of CO<sub>2</sub> during winter. All data are from the highest level available.

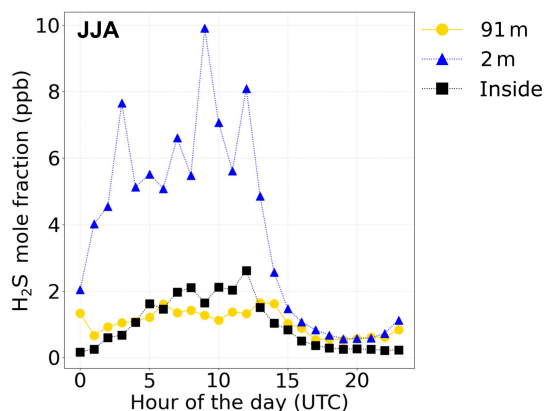


**Figure 6.** Diurnal cycle of H<sub>2</sub>S measured at the Hobbs site during the summer months (June, July, August).

magnitude of CO<sub>2</sub> enhancements did not (Fig. 9). There were, however, changes in enhancements related to the seasonality of the wind direction (Fig. 9). We did not expect to observe significant enhancements of CO<sub>2</sub> coming from the O&G basin, but some interesting patterns emerged. The observations revealed that at Notrees tower the enhancements were larger than 3 ppm with winds coming predominantly from south (Fig. 9b) and south-southwest directions (Fig. 9a). The Notrees enhancements also corroborate the en-

hancements observed at Fort Stockton, which has the largest enhancements to SSW during the summer; and during the winter, Fort Stockton has enhancements coming from the north, pointing to a possible source that is between Notrees and Fort Stockton. As for Carlsbad and Maljamar, during the summer, the enhancements are more isotropic, from NE to SSW, and the largest enhancements from both towers come from the directions of the city of Carlsbad. During the winter, Carlsbad, particularly, has a strong enhancement coming from the east.

Only one of the network towers has measurements of H<sub>2</sub>S during the summer, as stated above, and thus we cannot verify the seasonality of this dataset. However, the H<sub>2</sub>S enhancements obtained from the Hobbs tower at 91 m a.g.l., in the order of 2 ppb, indicate a potential source NE of the tower (Fig. 10). There is a patch of oil and gas wells 0.5–1.5 km to the east and northeast of the tower that may be the source of H<sub>2</sub>S. The enhancements computed from the 2 m a.g.l. inlet, not shown here, presented the same pattern as the 91 m a.g.l. and are, on average, 0.05 ppb larger than the enhancements at the top level. During the summer, the enhancements obtained from the inlet temporarily installed inside the building, on average, did not exceed 0.2 ppb, coming from the southeast.

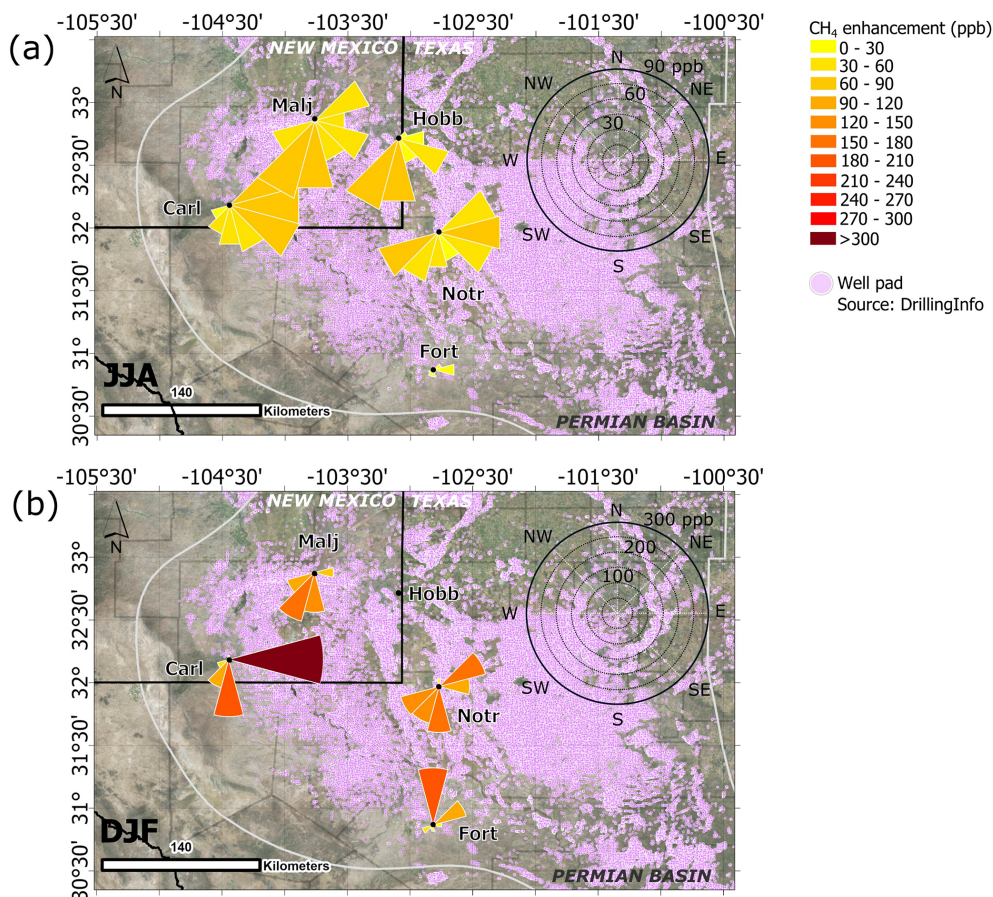


**Figure 7.** Methane enhancements at each tower location. The background for the figures indicates individual well locations for the Permian Basin. (a) CH<sub>4</sub> enhancements during summer months, i.e., June, July, August (JJA). (b) CH<sub>4</sub> enhancements during winter months, i.e., December, January, February (DJF). The “triangles” represent the mean of the afternoon (20:00–23:00 UTC) enhancements coming from the indicated direction. The gray boundary delimits the Permian Basin, while the black line is the boundary between New Mexico and Texas. Credits for base map: Esri, DigitalGlobe, GeoEye, Earthstar Geographics, CNES/Airbus DS, USDA, USGS, AeroGRID, IGN, and the GIS User Community.

#### 4.4 Isotopic ratio source signature

We used the Keeling plot approach (Keeling, 1961; Röckmann et al., 2016; Miles et al., 2018), determining the intercept of the best-fit line of the isotopic ratio as a function of the inverse methane mole fraction, to estimate the isotopic ratio of the methane source at the Maljamar tower. The intercepts of the best-fit lines for the peaks (Fig. 11) indicate that the sources contributing to the peaks have a mean isotopic ratio of  $-40.8 \pm 0.5\text{‰}$ . Oil and natural gas extraction is the only significant source of local methane in this region (Maasackers et al., 2016). The methane is lighter than that observed in the Marcellus region ( $-31.2\text{‰}$ ; Miles et al., 2018), and similar to that observed in the Barnett region ( $-41.8\text{‰}$ ; Milkov et al., 2020). The correlation coefficients were lower than that observed via a similar tower-based method in the Marcellus (Miles et al., 2018).

#### 5 Data availability

The data are available at The Pennsylvania State University Data Commons under DOI <https://doi.org/10.26208/98y5-t941> (Monteiro et al., 2021). We plan to update the data repository annually.

The dataset is organized by yearly data files and named by the host institution identification (PSU), the project identification (PERMIAN), type of measurements (INSITU), tower identification (e.g., CARLSBAD, HOBBS, FORTSTOCKTON, MALJAMAR, NOTREES), and year. The earliest files start on 1 March 2021.

In the datasets, the columns include location code, instrument serial number, inlet height (m a.g.l.), minimum time included in the hourly average (decimal day of year, UTC), maximum time included in the hourly average (decimal day of year, UTC), year, day of year, hour (UTC), calibrated CO<sub>2</sub> (dry mole fraction, ppm), standard deviation of the raw (2–

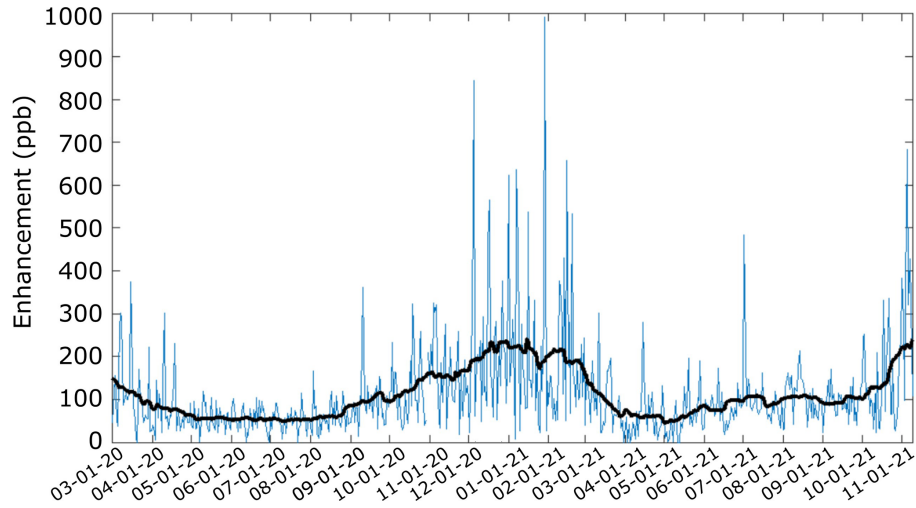


**Figure 8.** Daily afternoon differences (blue line) between the largest and smallest CH<sub>4</sub> mole fraction measured from the tower network from 1 March 2020 through 9 November 2021. Afternoon values are calculated by averaging measurements between 20:00–23:00 UTC. The black line indicates the 30 d running mean.

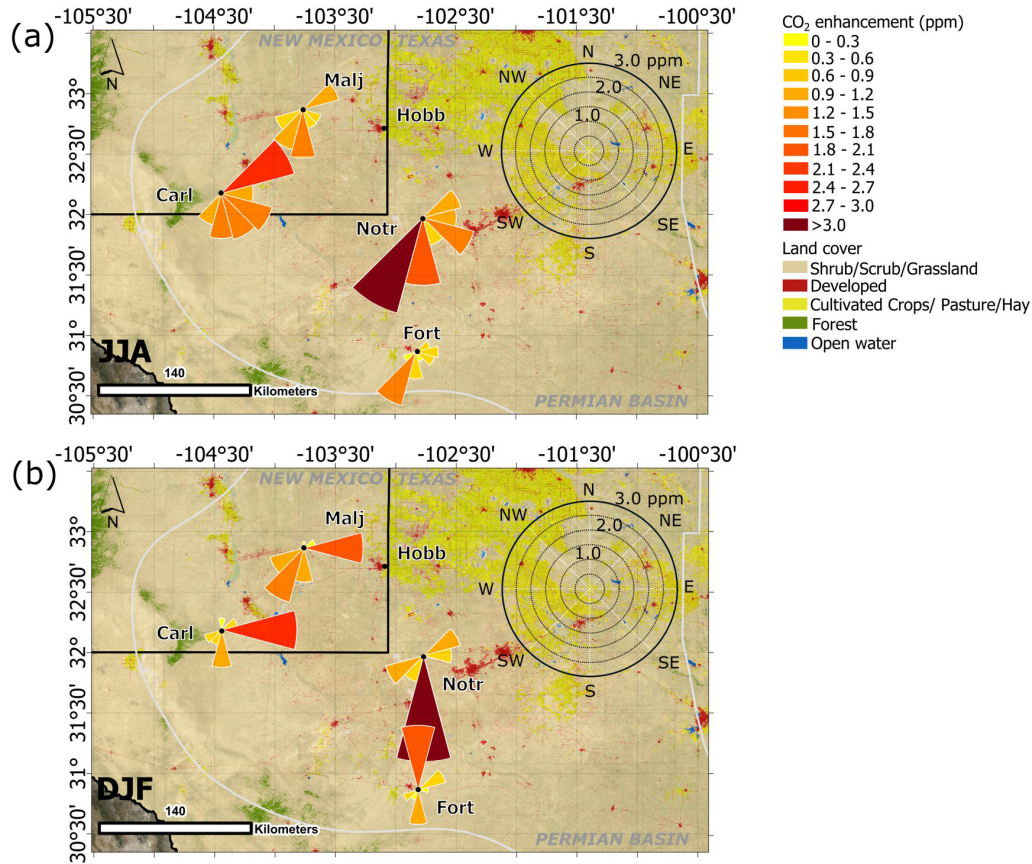


**Figure 9.** Carbon dioxide enhancements at each tower location. The background for the figures is the land cover from NLCD (National Land Cover Database; MRLC, 2019) for the Permian Basin. **(a)** CO<sub>2</sub> enhancements during summer months, i.e., June, July, August (JJA). **(b)** CO<sub>2</sub> enhancements during winter months, i.e., December, January, February (DJF). The “triangles” represent the mean of the afternoon (20:00–23:00 UTC) enhancements coming from the indicated direction. The gray boundary delimits the Permian Basin, while the black line is the boundary between New Mexico and Texas. Credits for base map: Esri, DigitalGlobe, GeoEye, Earthstar Geographics, CNES/Airbus DS, USDA, USGS, AeroGRID, IGN, and the GIS User Community.

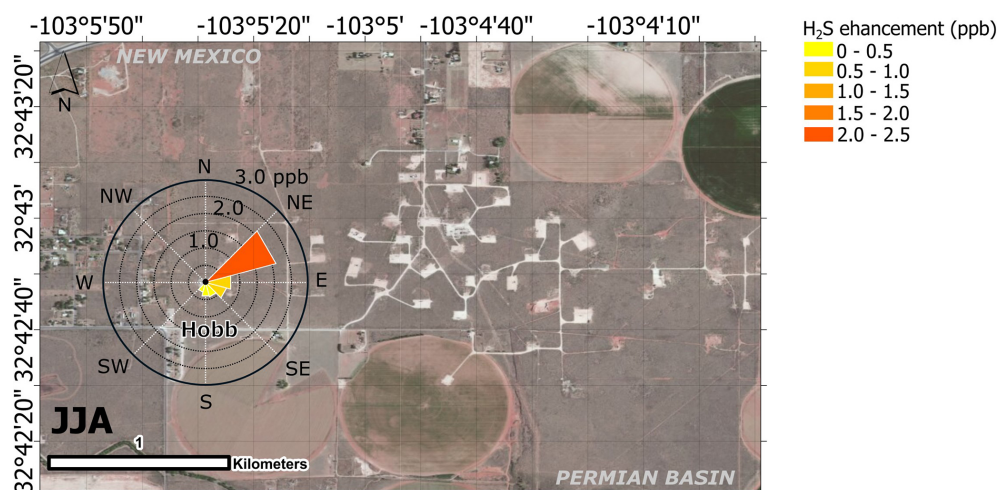


**Figure 10.** Hydrogen sulfide enhancements at the Hobbs tower, at 91 m a.g.l., during summer months, i.e., June, July, August (JJA). The “triangles” represent the mean of the afternoon (20:00–23:00 UTC) enhancements coming from the indicated direction. Credits for base map: Esri, DigitalGlobe, GeoEye, Earthstar Geographics, CNES/Airbus DS, USDA, USGS, AeroGRID, IGN, and the GIS User Community.

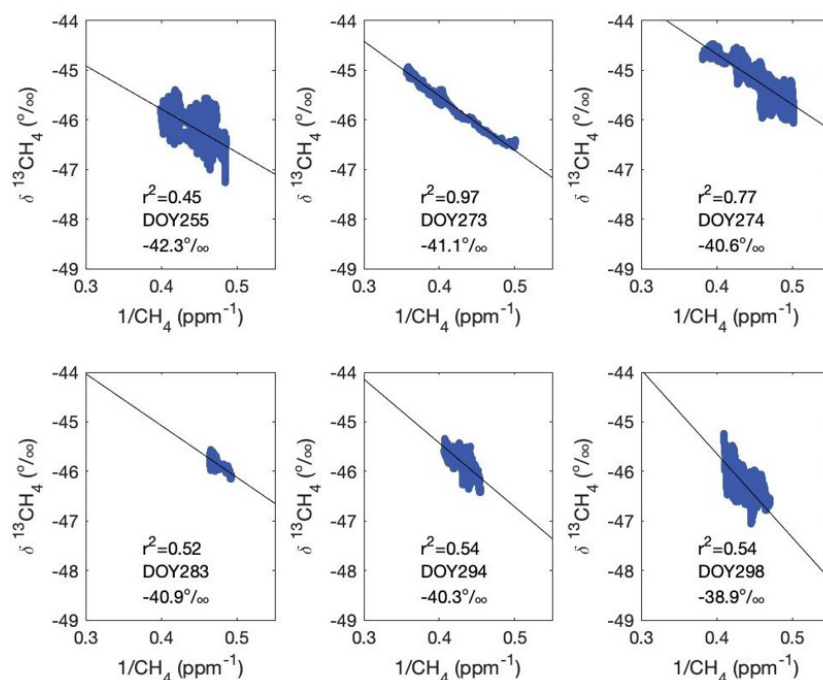


**Figure 11.** Keeling plots for six  $\text{CH}_4$  peaks measured at the Maljamar tower, using 10 min averaged data. Black lines indicate the best-fit lines. Correlation coefficients ( $r^2$ ), day of year (DOY), and y intercepts are indicated in the plots.

3 s)  $\text{CO}_2$  data within the hour (ppm), estimated  $\text{CO}_2$  uncertainty for that hour (ppm), calibrated  $\text{CH}_4$  (dry mole fraction, ppb), standard deviation of the raw (2–3 s)  $\text{CH}_4$  data within the hour (ppb), estimated  $\text{CH}_4$  uncertainty for that hour (ppb),  $\text{H}_2\text{S}$  (ppb) or  $\delta^{13}\text{CH}_4$  (‰) (depending on instrument type), standard deviation of the raw (2–3 s)  $\text{H}_2\text{S}$  or  $\delta^{13}\text{CH}_4$  data within the hour, estimated uncertainty for that

hour, and a user flag (1 means good; 0 means not recommended for use or not available).

Another sub-product of this dataset is the PermianMAP website, developed by EDF (PermianMAP, 2022), providing access to intermediate data products and a map of Permian Basin emissions, updated periodically.

## 6 Conclusions

The data presented show that regional tower networks can be operated to monitor methane emissions from O&G basins. Data quality and continuity successfully document regional methane enhancements associated with O&G production in the Delaware sub-basin of the Permian Basin. The location of upwind and downwind sites both change significantly as a function of season, illustrating the need to surround a basin with measurements. The magnitude of the enhancements also changes significantly vs. season, illustrating that accurate descriptions of boundary layer depths and winds are needed to interpret the data. A greater density of sites, more readily available instrument spares, or more reliable GHG measurement instruments could increase the data density, but the existing network performed sufficiently to document the basic characteristics of enhancements associated with this production basin. Basins with more complex methane background conditions and/or smaller emission rates may prove more challenging to characterize.

**Author contributions.** SJR and NLM collected data. BJH performed data ingestion and initial screening. NLM performed quality control, data processing, and uncertainty analysis. VCM performed data analysis and produced the majority of the figures. VCM and NLM wrote the article, with contributions from KJD, SJR, ZB, and BH. NLM, KJD, SJR, ZB, and DL designed the study.

**Competing interests.** The contact author has declared that neither they nor their co-authors have any competing interests.

**Disclaimer.** Publisher's note: Copernicus Publications remains neutral with regard to jurisdictional claims in published maps and institutional affiliations.

**Acknowledgements.** The tower network and modeling work was completed as part of the PermianMAP project, supported by the Environmental Defense Fund and its donors, including Bloomberg Philanthropies, Grantham Foundation for the Protection of the Environment, High Tide Foundation, the John D. and Catherine T. MacArthur Foundation, Quadrivium, and the Zegar Family Foundation. Computations for this research were performed on The Pennsylvania State University's Institute for Computational and Data Sciences' Roar supercomputer. We thank Carlsbad Caverns National Park for hosting an instrument.

**Financial support.** The PermianMAP project has been supported by the Environmental Defense Fund (award no. 224260) and its donors.

**Review statement.** This paper was edited by Nellie Elguindi and reviewed by two anonymous referees.

## References

- Allen, D. T., Smith, D., Torres, V. M., and Saldaña, F. C.: Carbon dioxide, methane and black carbon emissions from upstream oil and gas flaring in the United States, *Curr. Opin. Chem. Eng.*, 13, 119–123, <https://doi.org/10.1016/j.coche.2016.08.014>, 2016.
- Alvarez, R. A., Pacala, S. W., Winebrake, J. J., Chameides, W. L., and Hamburg, S. P.: Greater focus needed on methane leakage from natural gas infrastructure, *P. Natl. Acad. Sci. USA*, 109, 6435–6440, <https://doi.org/10.1073/pnas.1202407109>, 2012.
- Alvarez, R. A., Zavala-Araiza, D., Lyon, D. R., Allen, D. T., Barkley, Z. R., Brandt, A. R., Davis, K. J., Herndon, S. C., Jacob, D. J., Karion, A., Kort, E. A., Lamb, B. K., Lauvaux, T., Maasackers, J. D., Marchese, A. J., Omara, M., Pacala, S. W., Peischl, J., Robinson, A. L., Shepson, P. B., Sweeney, C., Townsend-Small, A., Wofsy, S. C., and Hamburg, S. P.: Assessment of methane emissions from the U. S. oil and gas supply chain, *Science*, 361, 186–188, <https://doi.org/10.1126/science.aar7204>, 2018.
- Andrews, A. E., Kofler, J. D., Trudeau, M. E., Williams, J. C., Neff, D. H., Masarie, K. A., Chao, D. Y., Kitzis, D. R., Novelli, P. C., Zhao, C. L., Dlugokencky, E. J., Lang, P. M., Croswell, M. J., Fischer, M. L., Parker, M. J., Lee, J. T., Baumann, D. D., Desai, A. R., Stanier, C. O., De Wekker, S. F. J., Wolfe, D. E., Munger, J. W., and Tans, P. P.: CO<sub>2</sub>, CO, and CH<sub>4</sub> measurements from tall towers in the NOAA Earth System Research Laboratory's Global Greenhouse Gas Reference Network: instrumentation, uncertainty analysis, and recommendations for future high-accuracy greenhouse gas monitoring efforts, *Atmos. Meas. Tech.*, 7, 647–687, <https://doi.org/10.5194/amt-7-647-2014>, 2014.
- Baray, S., Darlington, A., Gordon, M., Hayden, K. L., Leithead, A., Li, S.-M., Liu, P. S. K., Mittermeier, R. L., Moussa, S. G., O'Brien, J., Staebler, R., Wolde, M., Worthy, D., and McLaren, R.: Quantification of methane sources in the Athabasca Oil Sands Region of Alberta by aircraft mass balance, *Atmos. Chem. Phys.*, 18, 7361–7378, <https://doi.org/10.5194/acp-18-7361-2018>, 2018.
- Barkley, Z. R., Lauvaux, T., Davis, K. J., Deng, A., Miles, N. L., Richardson, S. J., Cao, Y., Sweeney, C., Karion, A., Smith, M., Kort, E. A., Schwietzke, S., Murphy, T., Cervone, G., Martins, D., and Maasackers, J. D.: Quantifying methane emissions from natural gas production in north-eastern Pennsylvania, *Atmos. Chem. Phys.*, 17, 13941–13966, <https://doi.org/10.5194/acp-17-13941-2017>, 2017.
- Barkley, Z. R., Lauvaux, T., Davis, K. J., Deng, A., Fried, A., Weibring, P., Richter, D., Walega, J. G., DiGangi, J., Ehrman, S. H., and Ren, X.: Estimating methane emissions from underground coal and natural gas production in South-western Pennsylvania, *Geophys. Res. Lett.*, 46, 4531–4540, <https://doi.org/10.1029/2019GL082131>, 2019a.
- Barkley, Z. R., Davis, K. J., Feng, S., Balashov, N., Fried, A., DiGangi, J., Choi, Y., and Halliday, H. S.: Forward modeling and optimization of methane emissions in the South Central United States using aircraft transects across frontal boundaries, *Geophys. Res. Lett.*, 46, 13564–13573, <https://doi.org/10.1029/2019GL084495>, 2019b.

- Barkley, Z. R., Davis, K. J., Feng, S., Cui, Y. Y., Fried, A., Weibring, P., Richter, D., Walega, J. G., Miller, S. M., Eckl, M., and Roiger, A.: Analysis of Oil and Gas Ethane and Methane Emissions in the Southcentral and Eastern United States Using Four Seasons of Continuous Aircraft Ethane Measurements, *J. Geophys. Res.-Atmos.*, 126, p.e2020JD034194, <https://doi.org/10.1029/2020JD034194>, 2021.
- Cambaliza, M. O. L., Shepson, P. B., Caulton, D. R., Stirm, B., Samarov, D., Gurney, K. R., Turnbull, J., Davis, K. J., Possolo, A., Karion, A., Sweeney, C., Moser, B., Hendricks, A., Lauvaux, T., Mays, K., Whetstone, J., Huang, J., Razlivanov, I., Miles, N. L., and Richardson, S. J.: Assessment of uncertainties of an aircraft-based mass balance approach for quantifying urban greenhouse gas emissions, *Atmos. Chem. Phys.*, 14, 9029–9050, <https://doi.org/10.5194/acp-14-9029-2014>, 2014.
- Carlson, K., Gerber, J., Mueller, N., Herrero, M., MacDonald, G. K., Brauman, K. A., Havlik, P., O'Connell, C. S., Johnson, J. A., Saatchi, S., and West, P. C.: Greenhouse gas emissions intensity of global croplands, *Nat. Clim. Change* 7, 63–68, <https://doi.org/10.1038/nclimate3158>, 2017.
- Caulton, D. R., Lu, J. M., Lane, H. M., Buchholz, B., Fitts, J. P., Golston, L. M., Guo, X., Li, Q., McSpirtt, J., Pan, D., and Wendt, L.: Importance of superemitter natural gas well pads in the Marcellus shale, *Environ. Sci. Technol.*, 53, 4747–4754, <https://doi.org/10.1021/acs.est.8b06965>, 2019.
- Chan, E., Worthy, D. E., Chan, D., Ishizawa, M., Moran, M. D., Delcloo, A., and Vogel, F.: Eight-year estimates of methane emissions from oil and gas operations in Western Canada are nearly twice those reported in inventories, *Environ. Sci. Technol.*, 54, 14899–14909, <https://doi.org/10.1021/acs.est.0c04117>, 2020.
- Conley, S., Franco, G., Faloona, I., Blake, D. R., Peischl, J., and Ryerson, T. B.: Methane emissions from the 2015 Aliso Canyon blowout in Los Angeles, CA, *Science*, 351, 1317–1320, <https://doi.org/10.1126/science.aaf2348>, 2016.
- Deighton, J. A., Townsend-Small, A., Sturmer, S. J., Hoschouer, J., and Heldman, L.: Measurements show that marginal wells are a disproportionate source of methane relative to production, *JAPCA J. Air Waste Ma.*, 70, 1030–1042, <https://doi.org/10.1080/10962247.2020.1808115>, 2020.
- Enverus Drillinginfo: Production, <https://app.drillinginfo.com/production> (last access: 12 March 2021), 2021.
- Heimbürger, A. M., Harvey, R. M., Shepson, P. B., Stirm, B. H., Gore, C., Turnbull, J., Cambaliza, M. O., Salmon, O. E., Kerlo, A. E. M., Lavoie, T. N., and Davis, K. J.: Assessing the optimized precision of the aircraft mass balance method for measurement of urban greenhouse gas emission rates through averaging, *Elementa: Science of the Anthropocene*, 5, 26, <https://doi.org/10.1525/elementa.134>, 2017.
- Iowa Environmental Mesonet of Iowa State University (IEM): ASOS Network, [https://mesonet.agron.iastate.edu/request/download.phtml?network=NM\\_ASOS](https://mesonet.agron.iastate.edu/request/download.phtml?network=NM_ASOS) (last access: 20 October 2021), 2021.
- IPCC (The Intergovernmental Panel on Climate Change): Climate Change 2021: The Physical Science Basis. Contribution of Working Group I to the Sixth Assessment Report of the Intergovernmental Panel on Climate Change, edited by: Masson-Delmotte, V., Zhai, P., Pirani, A., Connors, S. L., Péan, C., Berger, S., Caud, N., Chen, Y., Goldfarb, L., Gomis, M. I., Huang, M., Leitzell, K., Lonnoy, E., Matthews, J. B. R., Maycock, T. K., Waterfield, T., Yelekçi, O., Yu, R., and Zhou, B., Cambridge University Press, in press, 2021.
- Karion, A., Sweeney, C., Kort, E. A., Shepson, P. B., Brewer, A., Cambaliza, M., Conley, S. A., Davis, K., Deng, A., Hardesty, M., and Herndon, S. C.: Aircraft-based estimate of total methane emissions from the Barnett Shale region, *Environ. Sci. Technol.*, 49, 8124–8131, <https://doi.org/10.1021/acs.est.5b00217>, 2015.
- Karion, A., Callahan, W., Stock, M., Prinzivalli, S., Verhulst, K. R., Kim, J., Salameh, P. K., Lopez-Coto, I., and Whetstone, J.: Greenhouse gas observations from the Northeast Corridor tower network, *Earth Syst. Sci. Data*, 12, 699–717, <https://doi.org/10.5194/essd-12-699-2020>, 2020.
- Karion, A., Lopez-Coto, I., Gourdji, S. M., Mueller, K., Ghosh, S., Callahan, W., Stock, M., DiGangi, E., Prinzivalli, S., and Whetstone, J.: Background conditions for an urban greenhouse gas network in the Washington, DC, and Baltimore metropolitan region, *Atmos. Chem. Phys.*, 21, 6257–6273, <https://doi.org/10.5194/acp-21-6257-2021>, 2021.
- Keeling, C. D.: The Concentration and Isotopic Abundances of Carbon Dioxide in Rural and Marine Air, *Geochim. Cosmochim. Ac.*, 24, 277–298, 1961.
- Kirchgeßner, D. A., Piccot, S. D., and Masemore, S. S.: An improved inventory of methane emissions from coal mining in the United States, *JAPCA J. Air Waste Ma.*, 50, 1904–1919, <https://doi.org/10.1080/10473289.2000.10464227>, 2000.
- Lamb, B. K., Cambaliza, M. O., Davis, K. J., Edburg, S. L., Ferrara, T. W., Floerchinger, C., Heimbürger, A. M. F., Herndon, S., Lauvaux, T., Lavoie, T., Lyon, D. R., Miles, N., Prasad, K. R., Richardson, S., Roscioli, J. R., Salmon, O. E., Shepson, P. B., Stirm, B. H., and Whetstone, J.: Direct and indirect measurements and modeling of methane emissions in Indianapolis, Indiana, *Environ. Sci. Technol.*, 50, 8910–8917, <https://doi.org/10.1021/acs.est.6b01198>, 2016.
- Lin, J. C., Bares, R., Fasoli, B., Garcia, M., Crosman, E., and Lyman, S.: Declining methane emissions and steady, high leakage rates observed over multiple years in a western US oil/gas production basin, *Sci. Rep.-UK*, 11, 1–12, <https://doi.org/10.1038/s41598-021-01721-5>, 2021.
- Lyon, D. R., Hmiel, B., Gautam, R., Omara, M., Roberts, K. A., Barkley, Z. R., Davis, K. J., Miles, N. L., Monteiro, V. C., Richardson, S. J., Conley, S., Smith, M. L., Jacob, D. J., Shen, L., Varon, D. J., Deng, A., Rudelis, X., Sharma, N., Story, K. T., Brandt, A. R., Kang, M., Kort, E. A., Marchese, A. J., and Hamburg, S. P.: Concurrent variation in oil and gas methane emissions and oil price during the COVID-19 pandemic, *Atmos. Chem. Phys.*, 21, 6605–6626, <https://doi.org/10.5194/acp-21-6605-2021>, 2021.
- Maasakkers, J. D., Jacob, D. J., Sulprizio, M. P., Turner, A. J., Weitz, M., Wirth, T., Hight, C., DeFigueiredo, M., Desai, M., Schmeltz, R., and Hockstad, L.: Gridded national inventory of US methane emissions, *Environ. Sci. Technol.*, 50, 13123–13133, <https://doi.org/10.1021/acs.est.6b02878>, 2016.
- Maasakkers, J. D., Jacob, D. J., Sulprizio, M. P., Scarpelli, T. R., Nesser, H., Sheng, J.-X., Zhang, Y., Hersher, M., Bloom, A. A., Bowman, K. W., Worden, J. R., Janssens-Maenhout, G., and Parker, R. J.: Global distribution of methane emissions, emission trends, and OH concentrations and trends inferred from an inversion of GOSAT satellite data for 2010–2015, *Atmos.*

- Chem. Phys., 19, 7859–7881, <https://doi.org/10.5194/acp-19-7859-2019>, 2019.
- McKain, K., Down, A., Raciti, S. M., Budney, J., Hutyra, L. R., Floerchinger, C., Herndon, S. C., Nehrkorn, T., Zahniser, M. S., Jackson, R. B., and Phillips, N.: Methane emissions from natural gas infrastructure and use in the urban region of Boston, Massachusetts, *P. Natl. Acad. Sci. USA*, 112, 1941–1946, <https://doi.org/10.1073/pnas.1416261112>, 2015.
- Miles, N. L., Richardson, S. J., Lauvaux, T., Davis, K. J., Balashov, N. V., Deng, A., Turnbull, J. C., Sweeney, C., Gurney, K. R., Patarasuk, R., Razlivanov, I., Cambaliza, M. O. L., and Shepson, P. B.: Quantification of urban atmospheric boundary layer greenhouse gas dry mole fraction enhancements in the dormant season: Results from the Indianapolis Flux Experiment (INFLUX), *Elementa: Science of the Anthropocene*, 5, 27, <https://doi.org/10.1525/elementa.127>, 2017.
- Miles, N. L., Martins, D. K., Richardson, S. J., Rella, C. W., Arata, C., Lauvaux, T., Davis, K. J., Barkley, Z. R., McKain, K., and Sweeney, C.: Calibration and field testing of cavity ring-down laser spectrometers measuring CH<sub>4</sub>, CO<sub>2</sub>, and δ<sup>13</sup>CH<sub>4</sub> deployed on towers in the Marcellus Shale region, *Atmos. Meas. Tech.*, 11, 1273–1295, <https://doi.org/10.5194/amt-11-1273-2018>, 2018.
- Milkov, A. V., Schwietzke, S., Allen, G., Sherwood, O. A., and Etiope, G.: Using global isotopic data to constrain the role of shale gas production in recent increases in atmospheric methane, *Sci. Rep.-UK*, 10, 4199, <https://doi.org/10.1038/s41598-020-61035-w>, 2020.
- Mitchell, A. L., Tkacik, D. S., Roscioli, J. R., Herndon, S. C., Yacovitch, T. I., Martinez, D. M., Vaughn, T. L., Williams, L. L., Sullivan, M. R., Floerchinger, C., and Omara, M.: Measurements of methane emissions from natural gas gathering facilities and processing plants: Measurement results, *Environ. Sci. Technol.*, 49, 3219–3227, <https://doi.org/10.1021/es5052809>, 2015.
- Monteiro, V., Miles, N. L., Richardson, S. J., Barkley, Z. R., Haupt, B. J., and Davis, K. J.: Permian Basin: in-situ tower greenhouse gas data, *Data Commons*, Penn State [data set], <https://doi.org/10.26208/98y5-t941>, 2021.
- Moraes, L. E. and Fadel, J.: Minimizing environmental impacts of livestock production using diet optimization models, in: *Sustainable Animal Agriculture*, edited by: Kebreab, E., CABI, Boston, MA, 67–82, <https://doi.org/10.1079/9781780640426.0067>, 2013.
- Multi-Resolution Land Characteristics (MRLC) Consortium: National Land Cover Database (NLCD), <https://www.arcgis.com/home/item.html?id=3ccf118ed80748909eb85c6d262b426f> (last access: 15 October 2021), 2019.
- Occupational Safety and Health Administration (OSHA): Hydrogen Sulfide – Hazards, <https://www.osha.gov/hydrogen-sulfide/hazards> (last access: 6 January 2022), 2022.
- Ocko, I. B., Sun, T., Shindell, D., Oppenheimer, M., Hristov, A. N., Pacala, S. W., Mauzerall, D. L., Xu Y., and Hamburg, S. P.: Acting rapidly to deploy readily available methane mitigation measures by sector can immediately slow global warming, *Environ. Res. Lett.*, 16, 054042, <https://doi.org/10.1088/1748-9326/abf9c8>, 2021.
- Omara, M., Sullivan, M. R., Li, X., Subramanian, R., Robinson, A. L., and Presto, A. A.: Methane emissions from conventional and unconventional natural gas production sites in the Marcellus Shale Basin, *Environ. Sci. Technol.*, 50, 2099–2107, <https://doi.org/10.1021/acs.est.5b05503>, 2016.
- Pandey, S., Gautam, R., Houweling, S., Van Der Gon, H. D., Sadavarte, P., Borsdorff, T., Hasekamp, O., Landgraf, J., Tol, P., Van Kempen, T., and Hoogeveen, R.: Satellite observations reveal extreme methane leakage from a natural gas well blowout, *P. Natl. Acad. Sci. USA*, 116, 26376–26381, <https://doi.org/10.1073/pnas.1908712116>, 2019.
- PermianMAP: Permian methane analysis project, <https://permianmap.org/> (last access: 10 January 2022), 2022.
- Plant, G., Kort, E. A., Floerchinger, C., Gvakharia, A., Vimont, I., and Sweeney, C.: Large fugitive methane emissions from urban centers along the US East Coast, *Geophys. Res. Lett.*, 46, 8500–8507, <https://doi.org/10.1029/2019GL082635>, 2019.
- Qu, Z., Jacob, D. J., Shen, L., Lu, X., Zhang, Y., Scarpelli, T. R., Nesser, H., Sulprizio, M. P., Maasackers, J. D., Bloom, A. A., Worden, J. R., Parker, R. J., and Delgado, A. L.: Global distribution of methane emissions: a comparative inverse analysis of observations from the TROPOMI and GOSAT satellite instruments, *Atmos. Chem. Phys.*, 21, 14159–14175, <https://doi.org/10.5194/acp-21-14159-2021>, 2021.
- Rella, C. W., Chen, H., Andrews, A. E., Filges, A., Gerbig, C., Hatakka, J., Karion, A., Miles, N. L., Richardson, S. J., Steinbacher, M., Sweeney, C., Wastine, B., and Zellweger, C.: High accuracy measurements of dry mole fractions of carbon dioxide and methane in humid air, *Atmos. Meas. Tech.*, 6, 837–860, <https://doi.org/10.5194/amt-6-837-2013>, 2013.
- Richardson, S. J., Miles, N. L., Davis, K. J., Lauvaux, T., Martins, D. K., Turnbull, J. C., McKain, K., Sweeney, C., and Cambaliza, M. O. L.: Tower measurement network of in-situ CO<sub>2</sub>, CH<sub>4</sub>, and CO in support of the Indianapolis FLUX (INFLUX) Experiment, *Elementa: Science of the Anthropocene*, 5, 59, <https://doi.org/10.1525/elementa.140>, 2017.
- Robertson, A. M., Edie, R., Field, R. A., Lyon, D., McVay, R., Omara, M., Zavala-Araiza, D., and Murphy, S. M.: New Mexico Permian Basin measured well pad methane emissions are a factor of 5–9 times higher than US EPA estimates, *Environ. Sci. Technol.*, 54, 13926–13934, 2020.
- Röckmann, T., Eyer, S., van der Veen, C., Popa, M. E., Tuzson, B., Monteil, G., Houweling, S., Harris, E., Brunner, D., Fischer, H., Zazzeri, G., Lowry, D., Nisbet, E. G., Brand, W. A., Necki, J. M., Emmenegger, L., and Mohn, J.: In situ observations of the isotopic composition of methane at the Cabauw tall tower site, *Atmos. Chem. Phys.*, 16, 10469–10487, <https://doi.org/10.5194/acp-16-10469-2016>, 2016.
- Sargent, M., Barrera, Y., Nehrkorn, T., Hutyra, L. R., Gately, C. K., Jones, T., McKain, K., Sweeney, C., Colm, Hegarty, J., Hardiman, B., Wang, J. A., and Wofsy, S. C.: Anthropogenic and biogenic CO<sub>2</sub> fluxes in the Boston urban region, *P. Natl. Acad. Sci. USA*, 115, 7491–7496, <https://doi.org/10.1073/pnas.1803715115>, 2018.
- Sargent, M. R., Floerchinger, C., McKain, K., Budney, J., Gottlieb, E. W., Hutyra, L. R., Rudek, J., and Wofsy, S. C.: Majority of US urban natural gas emissions unaccounted for in inventories, *P. Natl. Acad. Sci. USA*, 118, e2105804118, <https://doi.org/10.1073/pnas.2105804118>, 2021.
- Saunio, M., Stavert, A. R., Poulter, B., Bousquet, P., Canadell, J. G., Jackson, R. B., Raymond, P. A., Dlugokencky, E. J., Houweling, S., Patra, P. K., Ciais, P., Arora, V. K., Bastviken, D., Berga-



- maschi, P., Blake, D. R., Brailsford, G., Bruhwiler, L., Carlson, K. M., Carrol, M., Castaldi, S., Chandra, N., Crevoisier, C., Crill, P. M., Covey, K., Curry, C. L., Etiope, G., Frankenberg, C., Gedney, N., Hegglin, M. I., Höglund-Isaksson, L., Hugelius, G., Ishizawa, M., Ito, A., Janssens-Maenhout, G., Jensen, K. M., Joos, F., Kleinen, T., Krummel, P. B., Langenfelds, R. L., Laruelle, G. G., Liu, L., Machida, T., Maksyutov, S., McDonald, K. C., McNorton, J., Miller, P. A., Melton, J. R., Morino, I., Müller, J., Murguia-Flores, F., Naik, V., Niwa, Y., Noce, S., O'Doherty, S., Parker, R. J., Peng, C., Peng, S., Peters, G. P., Prigent, C., Prinn, R., Ramonet, M., Regnier, P., Riley, W. J., Rosentreter, J. A., Segers, A., Simpson, I. J., Shi, H., Smith, S. J., Steele, L. P., Thornton, B. F., Tian, H., Tohjima, Y., Tubiello, F. N., Tsuruta, A., Viovy, N., Voulgarakis, A., Weber, T. S., van Weele, M., van der Werf, G. R., Weiss, R. F., Worthy, D., Wunch, D., Yin, Y., Yoshida, Y., Zhang, W., Zhang, Z., Zhao, Y., Zheng, B., Zhu, Q., Zhu, Q., and Zhuang, Q.: The Global Methane Budget 2000–2017, *Earth Syst. Sci. Data*, 12, 1561–1623, <https://doi.org/10.5194/essd-12-1561-2020>, 2020.
- Schwietzke, S., Sherwood, O. A., Bruhwiler, L. M., Miller, J. B., Etiope, G., Dlugokencky, E. J., Michel, S. E., Arling, V. A., Vaughn, B. H., White, J. W., and Tans, P. P.: Upward revision of global fossil fuel methane emissions based on isotope database, *Nature*, 538, 88–91, <https://doi.org/10.1038/nature19797>, 2016.
- Schwietzke, S., Pétron, G., Conley, S., Pickering, C., Mielke-Maday, I., Dlugokencky, E. J., Tans, P. P., Vaughn, T., Bell, C., Zimmerle, D., and Wolter, S.: Improved mechanistic understanding of natural gas methane emissions from spatially resolved aircraft measurements, *Environ. Sci. Technol.*, 51, 7286–7294, <https://doi.org/10.1021/acs.est.7b01810>, 2017.
- Turner, A. J., Jacob, D. J., Wecht, K. J., Maasackers, J. D., Lundgren, E., Andrews, A. E., Biraud, S. C., Boesch, H., Bowman, K. W., Deutscher, N. M., Dubey, M. K., Griffith, D. W. T., Hase, F., Kuze, A., Notholt, J., Ohyama, H., Parker, R., Payne, V. H., Sussmann, R., Sweeney, C., Velazco, V. A., Warneke, T., Wennberg, P. O., and Wunch, D.: Estimating global and North American methane emissions with high spatial resolution using GOSAT satellite data, *Atmos. Chem. Phys.*, 15, 7049–7069, <https://doi.org/10.5194/acp-15-7049-2015>, 2015.
- U.S. Environmental Protection Agency (U.S. EPA): Inventory of US greenhouse gas emissions and sinks: 1990–2017, U.S. Environmental Protection Agency, <https://www.epa.gov/ghgemissions/inventory-us-greenhouse-gas-emissions-and-sinks-1990-2017> (last access: 17 May 2022), 2019.
- Verhulst, K. R., Karion, A., Kim, J., Salameh, P. K., Keeling, R. F., Newman, S., Miller, J., Sloop, C., Pongetti, T., Rao, P., Wong, C., Hopkins, F. M., Yadav, V., Weiss, R. F., Duren, R. M., and Miller, C. E.: Carbon dioxide and methane measurements from the Los Angeles Megacity Carbon Project – Part 1: calibration, urban enhancements, and uncertainty estimates, *Atmos. Chem. Phys.*, 17, 8313–8341, <https://doi.org/10.5194/acp-17-8313-2017>, 2017.
- Wennberg, P. O., Mui, W., Wunch, D., Kort, E. A., Blake, D. R., Atlas, E. L., Santoni, G. W., Wofsy, S. C., Diskin, G. S., Jeong, S., and Fischer, M. L.: On the sources of methane to the Los Angeles atmosphere, *Environ. Sci. Technol.*, 46, 17, 9282–9289, <https://doi.org/10.1021/es301138y>, 2012.
- Yadav, V., Duren, R., Mueller, K., Verhulst, K. R., Nehr Korn, T., Kim, J., Weiss, F., Keeling, R., Sander, S., Fischer, M. L., Newman, S., Falk, M., Kuwayama, T., Hopkins, F., Rafiq, T., Whetstone, J., and Miller, C.: Spatio-temporally resolved methane fluxes from the Los Angeles Megacity, *J. Geophys. Res.-Atmos.: Atmospheres*, 124, 5131–5148, <https://doi.org/10.1029/2018JD030062>, 2019.
- Yver Kwok, C., Laurent, O., Gueuri, A., Philippon, C., Wastine, B., Rella, C. W., Vuillemin, C., Truong, F., Delmotte, M., Kazan, V., Darding, M., Lebègue, B., Kaiser, C., Xueref-Rémy, I., and Ramonet, M.: Comprehensive laboratory and field testing of cavity ring-down spectroscopy analyzers measuring H<sub>2</sub>O, CO<sub>2</sub>, CH<sub>4</sub> and CO, *Atmos. Meas. Tech.*, 8, 3867–3892, <https://doi.org/10.5194/amt-8-3867-2015>, 2015.
- Zhang, Y., Gautam, R., Pandey, S., Omara, M., Maasackers, J. D., Sadavarte, P., Lyon, D., Nesser, H., Sulprizio, M. P., Varon, D. J., Zhang, R., Houweling, S., Zavala-Araiza, D., Alvarez, R. A., Lorente, A., Hamburg, S. P., Aben, I., and Jacob, D. J.: Quantifying methane emissions from the largest oil-producing basin in the United States from space, *Sci. Adv.*, 6, eaaz5120, <https://doi.org/10.1126/sciadv.aaz5120>, 2020.